Simulation of unsteady separated flows using advanced statistical and hybrid turbulence modelling

Guillaume Martinat[1], Yannick Hoarau[2], Marianna Braza[1], and Daniel Ruiz[3]

[1] Institut de mécanique des fluides de Toulouse, Allée Camille de Soula,31000, Toulouse, France
[2] Intitut de mécanique des fluides et solides de Strasbourg
[3] Institut de Recherche en Informatique de Toulouse, France

Abstract. In this study, comparison are made between advanced statistical modelling, hybrid modelling and the experiement from Lienhardt and al (1) on the ahmed car body. Results are showing an slight improvement when using hybrid modelling however, all approaches are overestimating the detachment of the flow on the rear slant of the geometry.

1 Introduction

The context of this study is the evaluation of advanced turbulence modeling for three dimensional unsteady turbulent flows at high Reynolds number. Despite numerous studies, there is still no universal approach to model accurately such complex flows. Large eddy simulation is very efficient to model unsteady separated flow but remains unaffordable for high Reynolds number flows where classical URANS modelling is affordable but can't provide reliable results when a detachment occurs.
Because of the complexity of cars aerodynamics and in order to simplify studies, Ahmed car body has become reference geometry. Past experimental studies have shown that the topology of this complex fully three dimensional flow is dependant from the slant angle of the geometry considered. When the slant angle is below 30 degrees, the flow has an unsteady topology. Two vortices are created on the side edges of the slant. Over the slant, the flow separates and reattaches later on the slant. Two counter-rotating vortices are created on the rear face of the body. When the slant angle is above 30 degrees, the vortex over the slant doesn't reattach and is then more intense as the sides vortices. For this case, the flow remains steady. Figure 1 shows the evolution of average drag coefficient with the slant angle, we can notice the discontinuity in drag variation for slant angle above 30^o. In this study, we will concentrate on the 25^o slant angle geometries which are well documented DESIDER and Ercoftac test cases. The test case is based on experimental sudy from Lienhardt and al (1) where Reynolds number is 768000, based on the body height.
From the point of vue of turbulence modelling, the ahmed car body is a very tough test case, especially when considering the 25^o slant angle configuration

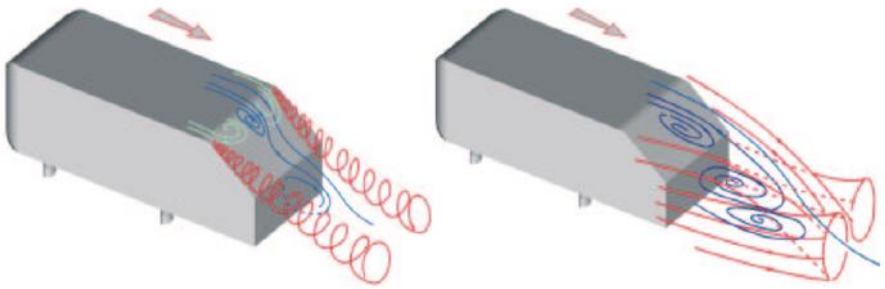

Fig. 1. Scheme of the flow topology observed and streaklines fo 25^o (left) and 35^o (right) slant angle, Lienhardt and al (1)

because of a highly three dimensional unsteady flow.
The aim of this study is to evaluate the performances of advanced URANS turbulence models (Organised Eddy Simulation and Scale Adaptative Simulation) compared to hybrid approaches (Detached and Delayed Detached Eddy Simulation) on the two test cases precited. First the turbulence approaches used and the flow solver will be described before analysing the results obtained on the 25^o slant angle ahmed car body.

2 Turbulence modelling : macrosimulation for unsteady flows

Averaged Navier-Stokes equation are considered according to the decomposition of Cantwell and Coles (2). Due to a non linear interaction of chaotic with organised structure, the slope of the fluctuation spectrum in the inertial part is different than the one of turbulence in equilibrium (Braza and al (3)). As a consequence, production is not equal to dissipation like in URANS equilibrium turbulence modelling, but instead we need to reconsider the turbulence time and length scales.

2.1 Organised Eddy Simulation (OES)

In this context of advanced URANS methods, EMT2-IMFT has developped the Organised Eddy simulation (O.E.S) approach (Braza and al (3)). This consists in distinguishing the structures to be resolved from the one to be modelled on the basis of their physical nature, organised or chaotic and not on their size (this is the case in LES approach). According to this approach, the turbulence spectrum, extended in the range from the low to the high wavenumbers, has to be modeled by reconsidering the turbulence scales of the URANS modelling. This is needed because of the non linear interaction between the coherent part

and the random turbulence in the inertial range, that modifies the shape and the slope of the spectrum.
From the second order moement closure DRSM (Launder and al (4)) a modified two equation model has been derived, where the turbulence length scales have been modified in the sense of evaluation of the C_μ eddy diffusion coefficient and of the damping turbulence law towards the wall (Hoarau and al (5) and Jin and Braza (6)). In addition, a tensorial OES eddy-viscosity model has been derived to capture the non-equilibrium turbulence (Bourguet and al (7)) where the C_μ eddy diffusion coefficient varies according to a directional criterion of stress-strain misalignment. Isotropic OES model yields a two-equation low Reynolds model (e.g. Chien (8)) and modification for OES are given by the following equations :

$$C_\mu = 0.02$$

$$f_\mu = 1 - exp(0.0002y^+ 0.000065y^{+2})$$

The advantages of this approach are the robustness at high Reynolds number wall bounded flows and the fact that the method is not intrinsically three-dimensional.
This model was validated in numerous static studies and has given good results (Bouhadji and al (9)).

2.2 Detached Eddy Simulation (DES)

As mentioned by Travin and al (10), "A Detached-Eddy Simulation is a three-dimensional numerical simulation using a single turbulence model, which functions as a sub-grid scale model in regions where the grid density is fine enough for a Large-Eddy Simulation, and as a Reynolds-Average model in regions where it is not". The DES length scale is chosen according to the following equation :

$$\tilde{d} = min(d, C_{DES}\Delta)$$

where C_{DES} is the DES constant calibrated by means of homogeneous, isotropic turbulence spectrum, Δ is the largest dimension of the elementary control volume cell, $\Delta = max(\Delta x, \Delta y, \Delta z)$ and d is the URANS lengthscale which is the distance to the nearest wall in the case of Spalart and Allmaras modelling and a distance homogeneous to $\frac{k^{3/2}}{\varepsilon}$ otherwise, for example, for a $k-\omega$ turbulence model, $d = \frac{\sqrt{k}}{\beta\omega}$ and is replace in the dissipative term of the transport equation of k by the test precited.
Therefore, the DES approach leads to an URANS computation in the near wall region and to a subgrid LES approach in the farther region, where the vortices detachment occurs . This approach is less dissipative than URANS thanks to the choice of the lengthscale that allows the increase of the dissipation term in the turbulence kinetic energy equation comparing to URANS.

2.3 Delayed detached eddy simulation (DDES)

In order to avoid a transition from URANS to LES in the boundary layer that could produce non physical artefacts, Spalart and al (11) introduces a modification of the r_d parameter of the Spalart-Allmaras model ((12)) involved in near-wall damping as follows :

$$r_d = \frac{\nu + \nu_t}{S_{ij}\kappa^2 d^2}$$

By adding ν on the numerator as a small parameter it is ensured that in high Reynolds flows r_d remains away from 0 in the near wall regions. Then a damping function has been suggested write $f_d = 1 - tanh[(8r_d^3)]$ which is 1 away from the wall an 0 in the near wall regions where $rd << 1$. Finally we have :

$$\tilde{d} = d - f_d max(0, d - C_{DES}\Delta)$$

If $fd = 0$, $\tilde{d} = d$ which yields to RANS modelling and if $fd = 1$, $\tilde{d} = min(d, C_{DES}\Delta)$ which yields to the classical DES modelling ((13)). The boundary layer is then shielded from a transition from URANS to LES and that transition is moved farther away from the wall in case of an excessive mesh refinement.

2.4 Scale Adaptative Simulation (SAS)

According to Menter (14), SAS approach represents a new class of the URANS modelling different from the usual URANS formulation, using a turbulence lengthscale adapted to the flow inhomogeneities. SAS is based on the use of a second scale in the source term f the turbulence model. In addition to standard momentum equation in the form of first velocity gradient, SAS models rely on a second scale, in the form of higher velocity gradient. According to this, SAS satisfies the following beaviour : it provides proper URANS performances in stable flow regions and allows the breakup of large unsteady structures into a turbulent spectrum.
the SAS model used in this study derives from Menter's $k-\omega$ Baseline-SST two equation model ((15)). Governing equation only differs from SST original model by adding the SAS source term Q_{SAS} in the ω transport equation. Q_{SAS} is then defined as follows :

$$Q_{SAS} = max\left[\rho\zeta_2\mathcal{K}S^2\left(\frac{L}{L_{vK}}\right) - C\frac{2\rho k}{\sigma_\Phi}max\left(\frac{|\nabla\omega|^2}{\omega^2}, \frac{|\nabla k|^2}{k^2}\right), 0\right]$$

Where L and L_{vK} are repectively lenghtscale of modelled turbulence and von Karman lengthscale. Those two lengthscales are explicitely defined in Menter (14). The model parameters in the SAS source term are $\zeta_2 = 3.51$,$\sigma_\Phi = 2/3$, and $C = 2$.

3 Flow solver

3.1 The governing equations

The solver used in this study is the NSMB sovler. This solver has been developed within an european research project between research etablishments (EPFL, KTH and CERFACS) and industrial partners (EADS Airbus, SAAB and CFS-Engineering). Since 2004, NSMB is developped and used in a small consortium composed of CFS Engineering, RUAG Aerospace, EPFL, ETHZ, IMFT, IMFS, the Technical University of München, the University of the Army in München and Astrium Space Transportation. The governing equations are the unsteady Navier-Stokes equations which describe the conservation of mass, momentum and energy. In 3D Cartesian coordinates (x, y, z), the Unsteady Compressible Navier Stokes Equations can be expressed in conservative form as

$$\frac{\partial}{\partial t}(W) + \frac{\partial}{\partial x}(f - f_v) + \frac{\partial}{\partial y}(g - g_v) + \frac{\partial}{\partial z}(h - h_v) = 0 \tag{1}$$

where t denotes the time. The state vector W is given by

$$\mathrm{W} = \begin{pmatrix} \rho \\ \rho u \\ \rho v \\ \rho w \\ \rho E \end{pmatrix} \tag{2}$$

and the convective fluxes are defined as

$$\mathrm{f} = \begin{pmatrix} \rho u \\ \rho u^2 + p \\ \rho uv \\ \rho uw \\ u(\rho E + p) \end{pmatrix}, \mathrm{g} = \begin{pmatrix} \rho v \\ \rho vu \\ \rho v^2 + p \\ \rho vw \\ v(\rho E + p) \end{pmatrix}, \mathrm{h} = \begin{pmatrix} \rho w \\ \rho wu \\ \rho wv \\ \rho w^2 + p \\ w(\rho E + p) \end{pmatrix} \tag{3}$$

Here ρ is the density, u, v and w are the cartesian velocity components, p is the pressure and E is the total energy. The viscous fluxes are defined as

$$\mathrm{f}_v = \begin{pmatrix} 0 \\ \tau_{xx} \\ \tau_{xy} \\ \tau_{xz} \\ (\tau U)_x - q_x \end{pmatrix}, g_v = \begin{pmatrix} 0 \\ \tau_{yx} \\ \tau_{yy} \\ \tau_{yz} \\ (\tau U)_y - q_y \end{pmatrix}, h_v = \begin{pmatrix} 0 \\ \tau_{zx} \\ \tau_{zy} \\ \tau_{zz} \\ (\tau U)_z - q_z \end{pmatrix} \tag{4}$$

with the shear stress tensor τ given by

$$\tau_{xx} = \frac{2}{3}\mu\left(2\frac{\partial u}{\partial x} - \frac{\partial v}{\partial y} - \frac{\partial w}{\partial z}\right)$$
$$\tau_{yy} = \frac{2}{3}\mu\left(-\frac{\partial u}{\partial x} + 2\frac{\partial v}{\partial y} - \frac{\partial w}{\partial z}\right)$$
$$\tau_{zz} = \frac{2}{3}\mu\left(-\frac{\partial u}{\partial x} - \frac{\partial v}{\partial y} + 2\frac{\partial w}{\partial z}\right)$$
$$\tau_{xy} = \tau_{yx} = \mu\left(\frac{\partial v}{\partial x} + \frac{\partial u}{\partial y}\right)$$
$$\tau_{xz} = \tau_{zx} = \mu\left(\frac{\partial w}{\partial x} + \frac{\partial u}{\partial z}\right)$$
$$\tau_{yz} = \tau_{zy} = \mu\left(\frac{\partial v}{\partial z} + \frac{\partial w}{\partial y}\right)$$

where μ is the viscosity (Stokes hypothesis). The viscous dissipation in the energy equation is calculated from

$$(\tau \mathrm{U})_x = \tau_{xx}u + \tau_{xy}v + \tau_{xz}w$$
$$(\tau \mathrm{U})_y = \tau_{yx}u + \tau_{yy}v + \tau_{yz}w$$
$$(\tau \mathrm{U})_z = \tau_{zx}u + \tau_{zy}v + \tau_{zz}w$$

and the heat flux due to conduction is calculated according Fourier's law,

$$\mathrm{q}_x = -k\frac{\partial T}{\partial x}$$
$$\mathrm{q}_y = -k\frac{\partial T}{\partial y}$$
$$\mathrm{q}_z = -k\frac{\partial T}{\partial z}$$

where T is the temperature and k the heat conductivity. For caloric perfect gas flows the viscosity, μ, can be calculated from Sutherland's law which for air at standard atmosphere states

$$\frac{\mu}{\mu_\infty} = \left(\frac{T}{T_\infty}\right)^{3/2}\frac{(T_\infty + S_1)}{(T + S_1)}$$

where μ_∞ is the viscosity at the reference temperature T_∞, and S_1 a constant, in general set to 110.3 for air. Assuming a constant Prandtl number (for air $Pr = 0.72$), the heat conductivity can then be found by

$$k = \mu c_p / Pr$$

The specific heats at constant volume and constant pressure are constant for a caloric perfect gas, and can be calculated from $\mathrm{c}_v = R/(\gamma - 1)$ and $\mathrm{c}_p = \gamma \mathrm{c}_v$ respectively, with $\gamma = 1.4$, and R the gasconstant, equal to 287 (J/kgK) for air. To close the system of equations the pressure p must be related to the state vector

W. This relation depends on the model used to describe the thermodynamic properties of the gas. For a caloric perfect gas this relation states

$$\mathrm{p} = \rho \mathrm{e}(\gamma - 1) = \rho \mathrm{c_v T}(\gamma - 1) = \rho \mathrm{RT} \tag{5}$$

where e is the internal energy. The internal and total energy are related by

$$\mathrm{e} = \mathrm{E} - \frac{1}{2}\left(\mathrm{u}^2 + \mathrm{v}^2 + \mathrm{w}^2\right) \tag{6}$$

Many numerical fluxes are available in the solver and will not be described here : Jameson's central schemes, Roe's and AUSM+ upwind schemes. High order estimates of upwind solutions are carried out through the Total Variation Diminishing (TVD) technique, i.e. variable extrapolation and slope limiters of the Monotonic Upwind Scheme for Conservayion Laws (MUSCL) method or with variable reconstruction with Lagrange polynomials of the Weighted Essential Non-Oscillatory (WENO) method.

The system of equation is solved using Dual-Time Stepping and the LUSGS method

3.2 Dual Time Stepping

After applying the second-order backward differencing time discretization to the Navier-Stokes equations, the following non-linear system of equations has to be solved at each time step:

$$\mathcal{H}(U^{n+1}) = (1+\xi)\frac{\Delta U^n}{n}V - \xi\frac{\Delta U^{n-1}}{n-1}V + \theta R^{n+1} + (1-\theta+\phi)R^n - \phi R^{n-1} = 0 \tag{7}$$

The starting point for the dual time-stepping approach is the unsteady residual $\mathcal{H}$ as defined in Eq. (7) to be used in the following system of ordinary differential equations:

$$V\frac{dU}{dt^*} + \mathcal{H}(U) = 0 \tag{8}$$

which is integrated in a fictitious time t^* until steady state is reached, i.e. a system of ordinary differential equations has to be solved for each physical time step . For this, any appropriate time integration method can be used such as explicit or implicit methods developed for stationary problems. Also here, explicit methods imply restrictions on the fictitious time step *.

Discretizing Eq. (8) in fictitious time using the backward Euler method yields:

$$\frac{V}{*}\frac{\Delta U^\nu}{} + \mathcal{H}(U^{n+1,\nu+1}) = 0 \tag{9}$$

where ν is the subiteration index and $\Delta U^\nu = U^{n+1,\nu+1} - U^{n+1,\nu}$. Linearizing the unsteady residual around the fictitious instant ν yields the following linear system:

$$\left(\frac{V}{*}I + \left.\frac{\mathcal{H}(U^{n+1})}{U^{n+1}}\right|^\nu\right)\Delta U^\nu = -\mathcal{H}(U^{n+1,\nu}) \tag{10}$$

which is formally equal to that in Eq. (12). Writing out the linearization gives:

$$\left(\frac{V}{*}I + (1+\xi)\frac{V}{\Delta t}I + \theta\left.\frac{\partial R}{\partial U}\right|^{\nu}\right)\Delta U^{\nu} = -\mathcal{H}(U^{n+1,\nu}) \tag{11}$$

which can be solved using the LU-SGS method.

3.3 The Lower-Upper Symmetric Gauss-Seidel (LU-SGS) Method

In the following subsection the LU-SGS scheme introduced originally by Yoon and Jameson (16) is presented. The scheme is based on a lower-upper factorization and a symmetric Gauss-Seidel relaxation. The governing equations are discretized separately in space and in time. This ensures that the steady state solution will be independent of the time discretization procedure and therefore independent of the time step. Linearizing the residual from Eq. (1) about the time level n leads to the following equation:

$$\left(\frac{V}{\Delta t}\,I + \frac{\partial R}{\partial W}\right)\,\Delta W = -R(W^n) \tag{12}$$

with I being the identity matrix. Eq. (12) represents a large sparse linear system which has to be solved at each time step. The term $\partial R/\partial W$ stands symbolically for the Jacobian matrices resulting from the linearization of the fluxes. The implicit scheme becomes the standard Newton's method when the time step Δt tends to infinity. Note that the left hand side (LHS) of Eq. (12), which is called the implicit operator, does not affect the accuracy of the steady state solution. It has a large influence on the damping properties and hence on the convergence rate of the scheme.

A direct method could be applied to solve the linear system which would require the inversion of a large sparse block banded matrix. However, numerical costs and storage requirements are prohibitive using this method. Instead, iterative methods are applied and/or approximations are made to the linear system itself.

The starting point is a diagonally dominant form of Eq. (12) in order to meet the stability requirements for the relaxation method. This can obtained by linearizing the numerical fluxes of a first order Steger and Warming flux vector splitting. Inserting in Eq. (12) gives the following linear system:

$$\begin{aligned}
&\left[\frac{V}{\Delta t}\,I + A^{+}_{i+1/2} - A^{-}_{i-1/2} + A^{+}_{j+1/2} - A^{-}_{j-1/2} + A^{+}_{k+1/2} - A^{-}_{k-1/2}\right]\Delta W_{i,j,k} + \\
&A^{-}_{i+1/2}\Delta W_{i+1,j,k} + A^{-}_{j+1/2}\Delta W_{i,j+1,k} + A^{-}_{k+1/2}\Delta W_{i,j,k+1} \; - \\
&A^{+}_{i-1/2}\Delta W_{i-1,j,k} - A^{+}_{j-1/2}\Delta W_{i,j-1,k} - A^{+}_{k-1/2}\Delta W_{i,j,k-1} \;=\; -R(W^n)_{i,j,k}
\end{aligned} \tag{13}$$

where the split Jacobian matrix in the term $A^-_{i+1/2}\Delta W_{i+1,j,k}$ is evaluated at the cell side $i+1/2$ using the state vector in cell $i+1,j,k$. Note that the flux vector splitting used for the derivation of the LHS in Eq. (13) is not applied to the explicit residual $R(W^n)_{i,j,k}$.

Instead of calculating the split Jacobian matrices explicitly, Yoon and Jameson (16) use the following approximation:

$$A^{\pm} = \frac{1}{2}\left(A \pm r_A I\right) \tag{14}$$

with

$$r_A = \kappa \max\left(|\,\lambda_A\,|\right) \tag{15}$$

where λ_A represents eigenvalues of the Jacobian matrix A. The convergence and stability properties can be controlled with the constant κ which is greater than or equal to one (Blazek (17)). Further simplifications can be introduced into the implicit operator of Eq. (13) by writing

$$(A^+_{i+1/2} - A^-_{i-1/2})_{i,j,k} = (\tilde{r}_A)_{i,j,k}\, I \tag{16}$$

where $\tilde{r}_A$ is evaluated at the cell center according to Eq. (15) using the mean surface vector $1/2\,(\mathbf{s}_{i+1/2} - \mathbf{s}_{i-1/2})$. To avoid the explicit computation of A the terms $A^{\pm}\Delta W$ in Eq. (13) are replaced by:

$$A^{\pm}\,\Delta W = \frac{1}{2}\left(\Delta F \pm r_A\,\Delta W\right) \tag{17}$$

where ΔF denotes the time increment of the convective flux.

The LU-SGS method is best presented by decomposing the implicit operator in Eq. (13) into a sum of three matrices:

$$(E + D + F)\,\Delta W = -R^n \tag{18}$$

where

$$\begin{aligned}
E &= (A^+_{i-1/2})_{i-1,j,k} - (A^+_{j-1/2})_{i,j-1,k} - (A^+_{k-1/2})_{i,j,k-1} \\
F &= (A^-_{i+1/2})_{i+1,j,k} + (A^-_{j+1/2})_{i,j+1,k} + (A^-_{k+1/2})_{i,j,k+1} \\
D &= \frac{V}{\Delta t}\, I + (A^+_{i+1/2} - A^-_{i-1/2} + A^+_{j+1/2} - A^-_{j-1/2} + A^+_{k+1/2} - A^-_{k-1/2})_{i,j,k}
\end{aligned} \tag{19}$$

Here, E contains only the lower triangular part, F the upper triangular part and D the main diagonal of the implicit operator. System (18) can be inverted by applying a Symmetric Successive Over Relaxation (SSOR) method. The method sweeps through the mesh on planes with $i+j+k = const$, the so called oblique planes. The SSOR method performs two sweeps per iteration, one forward and one backward sweep. In operator form this can be written as (18):

$$\begin{aligned}(E+D)\,\Delta W^{k+1/2} &= -R^n - F\,\Delta W^k \\ (F+D)\,\Delta W^{k+1} &= -R^n - E\,\Delta W^{k+1/2}\end{aligned} \tag{20}$$

where k denotes the iteration index. By sweeping on the oblique planes, the off-diagonal terms $E\Delta W^{k+1/2}$ and $F\Delta W^k$ respectively become known and are added to the right hand side. As a consequence, only a block diagonal matrix has to be inverted. If the approximation of Eq. (16) is introduced, the implicit operator can be even reduced to a scalar diagonal matrix. The LU-SGS method is obtained when the LHS of Eq. (18) is factorized as follows (17):

$$(E+D)\,D^{-1}\,(F+D)\,\Delta W = -R^n \tag{21}$$

The LU-SGS scheme is now inverted by a forward and a backward sweep:

$$\begin{aligned}(E+D)\,\Delta W^* &= -R^n \\ (F+D)\,\Delta W &= D\,\Delta W^*\end{aligned} \tag{22}$$

The sweeps are accomplished in exactly the same way as already described for the SSOR method. Indeed, rewriting Eq. (22) by substituting $D\,\Delta W^* = -R^n - E\,\Delta W^*$ leads to the following form of the LU-SSOR scheme:

$$\begin{aligned}(E+D)\,\Delta W^* &= -R^n \\ (F+D)\,\Delta W &= -R^n - E\,\Delta W^*\end{aligned} \tag{23}$$

By comparison of Eq. (23) with Eq. (20) it can easily be seen that the LU-SGS method corresponds formally to the SSOR method if only one forward and one backward sweep is performed and if the initial solution is set to $\Delta W^0 = 0$. In order to to solve the linear system more accurately, the standard SSOR relaxation method has also been implemented in the code and the number of iterations can be specified by the user. Specifying one iteration means one forward and one backward sweep and corresponds to the LU-SGS scheme. Performing more than one Gauss-Seidel sweep improves the convergence rate particularly for high cell aspect ratio grids. Numerical experiments will show that for certain test cases the performance of the algorithm can be improved by using multiple sweeps.

As the time step $\Delta t \to \infty$, the LU-SSOR method reduces to an approximate Newton's method. Using a large time increment might lead to divergence since it is not ensured that the initial solution lies within the radius of convergence of the Newton's method. Also, the mismatch between the implicit and explicit operator might give a restriction on the time step. On the other hand, a small time step increases the diagonal dominance of the implicit operator and the system will be more robust, but at the expense of slower convergence.

The extension of the steady LU-SGS method to dual-time stepping is straightforward and consists in including the fictitious time step, the factors $(1+\xi)$ and θ in the implicit operator and adding source terms to the right hand side.

NSMB is parallelised using Message Passing Interface MPI. The multibloc decompostion of the structured grid is used for loadbalancing. The exchange of data between different nodes is done at the block interfaces.

4 Flow in the wake of the Ahmed car body

4.1 Grids used and numerical configuration

The case studied is based on the experiment from Lienhardt and al (1). The grid used is provided by Chalmers in the context of the DESIDER European program. It is composed with an O topology near wall in order to ensure cells orthogonality a C topology is used farther. The mesh is also composed of 3.6 million nodes dispached in 78 blocks. Time step is 0.05, space scheme is central fourth order and time scheme is an implicit backwards second order with dual time stepping.

4.2 Results

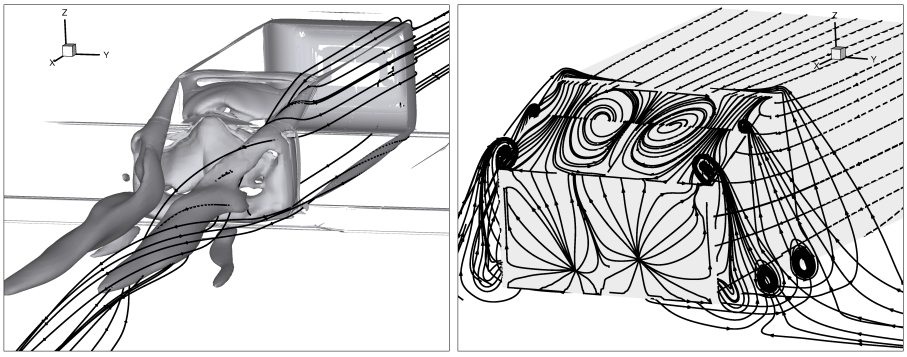

Fig. 2. *Isosurface of Q criterion (Q=20) and streamlines*

Flow topology observed The flow topology obtained was the same for the four different turbulence model used. Contrary to what was observed by Krajnovic (19), the detachment of the flow on the front part of the body is not predicted. Four longitudinal vortices are predicted, the two first on the lower side edges of the body are due to the ground effect and the two other are attached on the upper sied edges of the slant. Those vortices are pairing on each side in the wake of the Ahmed body (figure 4.2).
The flow detaches on the first edge of the slant and does not reattaches on the contrary of what was observed in Lienhardt experiments.

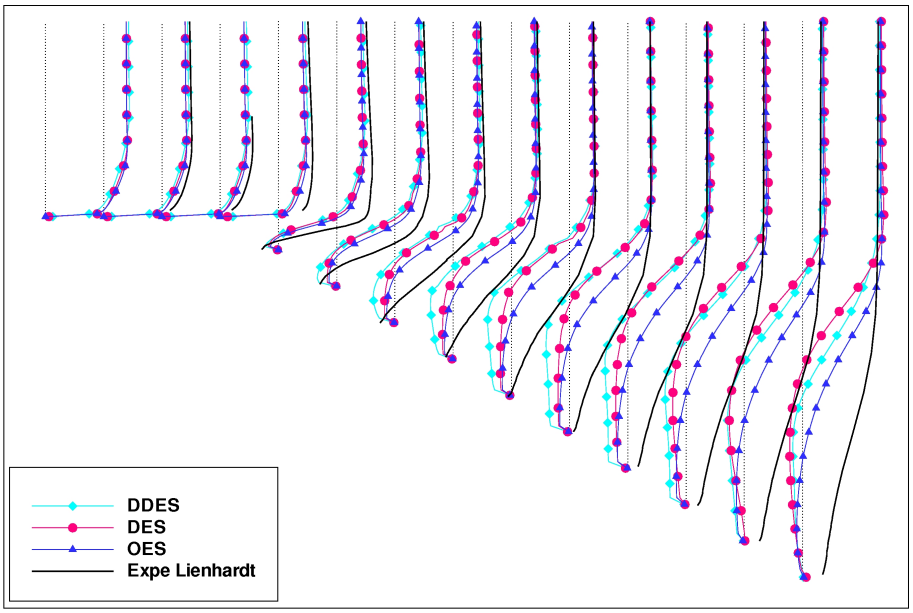

Fig. 3. *Longitudinal velocity profiles on the slant of the Ahmed body*

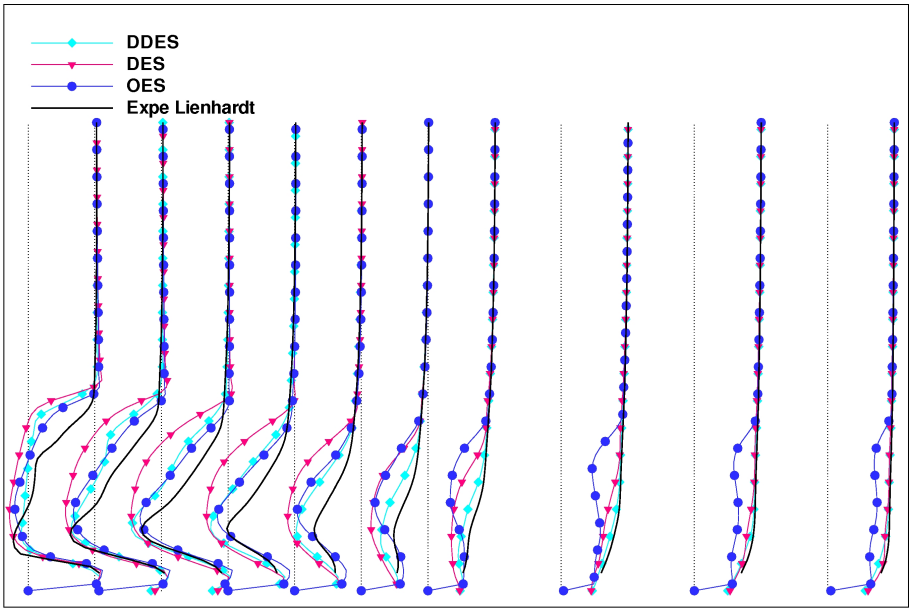

Fig. 4. *Longitudinal velocity profiles in the wake of the Ahmed body*

Comparison with experimental results For the four turbulence models, we can observe an overestimation of the flow detachment on the slant with no prediction of the reattachment. However, we can observe that OES modelling provides slightly better results on the slant than hybrid approaches due to a more efficient model near wall whereas hybrid approaches are far more efficient in the wake of the body thanks to their LES-like behaviour far from walls.
However, it seems that turbulence modelling has only a small effect on the results obtained which are quite close. This could be due to the unpredicted separated area on the front of the geometry that could produce a different developement of the boundary layer which in the case of statistical modelling would become more sensitive to adverse pressure gradient and then would produce an overestimateed detachment. a second hypothesis would be that a 3.6 million nodes mesh is still too coarse and a a more refined mesh especially on the first edge of the slant and on the front of the body could be needed.

5 Conclusion

In this study we evaluate the performances of four turbulence models on a complex unsteady turbulent flow : the ahmed car body. The 25^o slant angle geometry remains a tough test case that is still unpredicted with statistical approaches nowadays.
All the turbulence model used are overestimating the detachment of the flow even if DDES and OES approaches are showing promising behaviour.

Bibliography

[1] Lienhardt, H., Stoots, C., Becker, S.: Lda measurement of the flow and turbulent structures in the wake of a simplified car model. SAE Paper (2003-01-0656) (2000)

[2] Cantwell, B., Coles, D.: An experimental study of entrainment and transport in the turbulent near wake of a circular cylinder. J. Fluid Mech. **136** (1983) 321–374

[3] Braza, M., Perrin, R., Hoarau, Y.: Turbulence properties in the cylinder wake at high Reynolds number. J. Fluids Struct. **22** (2006) 757–771

[4] Launder, B., Reece, G., Rodi, W.: Progress in the development of a Reynolds stress turbulence closure. J. Fluid Mech. **68** (1975) 537–566

[5] Hoarau, Y., Braza, M., Tzabiras, G., Allain, C., Berton, E., Favier, D., Maresca, C.: Prediction of turbulent unsteady aerodynamic flows with a pronounced periodic character. In: IUTAM Symposium on Unsteady Separated Flows, Toulouse, France (2002)

[6] Jin, G., Braza, M.: A two-equation turbulence model for unsteady separated flows around airfoils. AIAA Journal **32** (1994) 2316–2320

[7] Bourguet, R., Braza, M., Perrin, R., Harran, G.: Anisotropic eddy-viscosity concept for strongly detached unsteady flows. AIAA Journal **45** (mai 2007) 1145–1149

[8] Chien, K.: Predictions of channel and boundary-layer flows with a low-Reynolds number turbulence model. AIAA Journal **20** (1982) 33–38

[9] Bouhadji, A., Bourdet, S., Braza, M., Hoarau, Y., Rodes, P., G.Tzabiras: Turbulence modelling of unsteady flows with a pronounced periodic character. Notes on Num. Fluid Mech. and Multidisciplinary Design **81** (2002) 87–96 dedicated volume in "Progress in Computational Flow-Structure Interaction".

[10] Travin, A., Shur, M., Strelets, M., Spalart, P.: Detached-Eddy Simulations past a Circular Cylinder. Flow, Turbulence and Combustion **63** (2000) 293–313

[11] Spalart, P., Deck, S., Shur, M., Squires, K., Strelets, M., Travin, A.: A new version of detached eddy simulation, resistant to ambiguous grid densities. Journal of theoretical and computational fluid dynamics **20** (2006) 181–195

[12] Spalart, P., Allmaras, S.: A one-equation turbulence models for aerodynamic flows. AIAA paper (92-0439) (1992) 30^{th} Aerospace Sciences Meeting - Reno, Nevada.

[13] Spalart, P., Jou, W.H., Strelets, M., Allmaras, S.R.: Comments on the feasibility of LES for wings, and on a hybrid RANS/LES approach. In: First AFOSR International Conference on DNS/LES, Aug. 4-8, Ruston, Louisiana (1997)

[14] Menter, F., Egorov, Y.: Development and application of sst-sas turbulence model in the desider project. In: Proceeding of the 2nd Hybrid RANS-LES Symposium, Corfu, Greece, June 17/18, 2007., Elsevier (2007)

[15] Menter, F.R.: Zonal two equation $k-\omega$ turbulence models for aerodynamics flows. AIAA Paper **93-2906** (1993)
[16] Yoon, S., Jameson, A.: A multigrid lu-ssor scheme for approximate newton iteration applied to the euler equations. NASA-CR-179524 (1986)
[17] Blazek, J.: Investigations of the implicit lu-ssor scheme. DLR-FB 93-51 (1993)
[18] Venkatakrishnan, V.: Implicit schemes and parallel computing in unstructured grid cfd. VKI LS 1995-02, Computational Fluid Dynamics (1995)
[19] Krajnovic, S., Davidson, L.: Flow around a simplified car, part 1 : Large eddy simulation. Journal of Fluids engineering (127) (2005)